Fracture-network analysis of the Latemar Platform (northern Italy): integrating outcrop studies to constrain the hydraulic properties of fractures in reservoir models

Herman Boro[1*], Enrique Rosero[2] and Giovanni Bertotti[1,3]

[1]*Dept. of Tectonic & Structural Geology, VU University Amsterdam, De Boelelaan 1051, 1081HV Amsterdam, The Netherlands*

[2]*ExxonMobil Upstream Research Company, P.O. Box 2189, Houston, TX 77252, USA*

[3]*Dept. of Geotechnology, Delft University of Technology Stevinweg 1, 2628CN, Delft, The Netherlands*

**Corresponding author (e-mail: herman.boro@sgs.com)*

ABSTRACT: Fractures in subsurface reservoirs are known to have significant impacts on reservoir productivity. Quantifying their importance, however, is challenged by limited subsurface observations, and intense computations for modelling and upscaling. In this paper, we present a workflow to construct and upscale fracture models based on outcrop studies in the Latemar carbonate platform (northern Italy). Fractures were first analysed to investigate their distinct characteristics throughout different sedimentological domains; that is, slope, margin and platform interior. Several fracture models were then built to represent different domains and were used to upscale fracture-network properties. Small-scale models were preferred to the reservoir-scale ones to enable multiple realizations and various sensitivity analyses in a time-efficient manner.

The fracture characteristics of the Latemar Platform vary across different sedimentological domains. This variation results in a non-homogeneous permeability field that will influence flow behaviours. Fractures in the slope domain are typically tall but low in intensity, resulting in relatively low effective permeabilities. In the platform interior, smaller sizes of fractures combined with higher intensities give rise to higher effective permeabilities. In general, fracture intensities, aperture and their intrinsic permeability would have a significant impact on the permeability field. Fracture shape and orientations are more important in affecting the connectivity.

INTRODUCTION

In carbonate reservoirs, the permeability field is commonly influenced by the presence of fracture networks (e.g. Cappa *et al.* 2005). Depending on their characteristics (e.g. open or closed), fractures can behave as fluid conduits or complete barriers, and, in some cases, combined conduits–baffles (Antonellini & Aydin 1995; Fisher & Knipe 2001; Billi *et al.* 2003). Detailed fracture characterization then becomes crucial in order to improve our ability to predict the flow behaviour in subsurface reservoirs (e.g. Wennberg *et al.* 2006; Storti *et al.* 2011).

Investigations of fluid flow through a fractured carbonate commonly employ a dual continuum model (e.g. Waren & Root 1963; Nardon *et al.* 1991; Manrique *et al.* 2007). In such a model, the matrix and fractures are considered to be two separate media, the interactions between the two during fluid flow simulations being defined by transfer functions (e.g. Kazemi *et al.* 1992). Correspondingly, the hydraulic properties for the matrix and fractures are assigned separately in the reservoir model.

To populate the reservoir model, the hydraulic properties of the matrix are commonly derived from direct measurements on reservoir rocks (e.g. Bennett *et al.* 1990; Parra *et al.* 2003). In contrast, hydraulic properties of fractures are best estimated from fracture-network realizations and upscaling (Kfoury *et al.* 2006; Rodriguez *et al.* 2006; Kozubowski *et al.* 2008) or from well productivity (Niemi *et al.* 2000; Cappa *et al.* 2005). Correspondingly, two main challenges are evident in estimating the hydraulic properties of fractures for subsurface reservoirs. First, fractures are usually observed only in well data such as cores and image logs (e.g. Iverson 1992; Narr *et al.* 2008; Li *et al.* 2011). The limited observations that are possible in the subsurface prevent a complete picture of the overall fracture distribution and the geometric characteristics of the fractures; that is, height, length, aperture and shape. In many instances, fractures in the reservoir model are simplified through subjective operations that might overlook the geological controls on fracture distributions (e.g. Casciano *et al.* 2004; Hui *et al.* 2007). Second, fracture modelling and upscaling processes are computationally intensive and time-consuming, especially for a reservoir-scale model (Kasiri & Bashiri 2011).

To address the problem of fracture sampling in reservoirs, outcrop studies should be integrated in developing a fracture model (Yose *et al.* 2001; Meurer *et al.* 2005; De Keijzer *et al.* 2007). In contrast with the subsurface data, outcropping reservoir

Petroleum Geoscience, Vol. **20**, 2014, pp. 79–92
http://dx.doi.org/10.1144/petgeo2013-007
Published *Online First* on January, 27, 2014

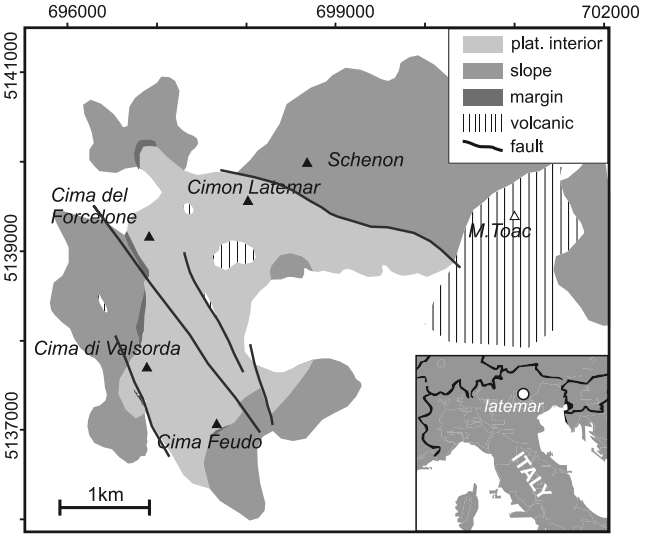

Fig. 1. Simplified facies map of the Latemar Platform, with the inset figure showing its location inside the Dolomites region of northern Italy.

analogues provide clear information on fracture geometry, distribution, and, more importantly, their relationship to geological features (e.g. bedding planes, stylolites and faults) and controlling factors (e.g. bedding thickness, rock types and structural positions) (e.g. Cooke & Underwood 2001; Underwood *et al.* 2003). It is important to note that fractures in the outcrop might have been affected by surface processes like weathering and stress release. The overall analysis, however, can help to constrain possible scenarios on fracture populations that may be relevant for the subsurface reservoir.

In this paper, we present a workflow for fracture-network modelling and upscaling procedures for reservoir-scale models. The adopted workflow combines a robust analysis of fracture-network characterizations derived from outcrop observations and the efficiency of small-scale fracture models for the computations. Similar to previous studies (e.g. Yose *et al.* 2001; Ruvo *et al.* 2003; Casciano *et al.* 2004), smaller-scale fracture models are preferable to models constructed at the scale of the reservoir. In our approach, the small-scale fracture model enables multiple realizations that offer important insights to the impacts of various uncertainties in fracture parameters and the stochastic approach during fracture realizations. In addition, with a small-scale model, we are able to integrate a distribution of important geological features, particularly those that have significant controls on fracture populations, such as bedding and lithology.

For this study, extensive fracture characterizations performed on the outcropping Latemar Platform have been used to constrain the design of our models (Boro *et al.* 2013). Based on our results, we will show how fracture-network characteristics impact distinct flow behaviours associated with different sedimentological domains across the Latemar Platform.

STRUCTURAL SETTING OF THE LATEMAR PLATFORM

The Latemar Platform is one of the isolated carbonate platforms developed in the Dolomites region of northern Italy (Fig. 1). The platform was deposited during Ladinian time, on the western margin of the Tethys Ocean (Goldhammer & Harris 1989; Egenhoff *et al.* 1999). The post-depositional subsidence of the platform is not well documented owing to the scarcity of Jurassic and younger sediments in the region. It is estimated that the platform could have reached a depth of approximately 2000 m (Rantitsch 1997; Emmerich *et al.* 2005) prior to the Alpine orogeny that brought the entire Dolomite region to its present-day elevation.

The Latemar Platform is renowned for its well-preserved carbonate successions that escaped regional dolomitization (Carmichael *et al.* 2008), and has been the focus of numerous sedimentological investigations in the past (e.g. Goldhammer & Harris 1989; Harris 1994; Marangon *et al.* 2011). The entire platform occupies a near-semi-circular area of 3×5 km, and its topography is characterized by a series of high peaks and deep gorges. The overall thickness of the Latemar Platform is estimated to be around 700–800 m (Egenhoff *et al.* 1999; Emmerich *et al.* 2005). A study by Preto *et al.* (2011) suggests a primary horseshoe shape for the overall geometry of the platform, affected by complex syndepositional faulting. The lateral and vertical growth of the Latemar Platform is mainly characterized by major aggradation (Emmerich *et al.* 2005). In contrast to other Ladinian platforms in the region (Bosellini 1984), such as the Sella and Rosengarten, extensive late-stage progradation is not well documented.

Typical for isolated carbonate platforms, the Latemar Platform comprises three first-order sedimentological domains – slope, margin and platform interior – characterized by different bedding arrangement and lithology. Slope sediments are dominated by coarse and massive grainstones, deposited with a primary dip of 30º. Sediments in the margin are also massive, dominated by boundstone formations with abundant microbial cements (Emmerich *et al.* 2005). The margin in the Latemar Platform is, however, thin and discontinuous due to syndepositional collapse (Emmerich *et al.* 2005). In the platform interior, well-stratified grainstone–mudstone layers are well developed and constrained within layers <3 m thick. The grain content for sediments inside the platform interior generally increases towards the margin (Egenhoff *et al.* 1999). Three tepee-abundant units are observed in the interior platform (e.g. Goldhammer *et al.* 1993; Egenhoff *et al.* 1999; Emmerich *et al.* 2005).

In recent years, structural studies have been performed on the platform focusing on different scales of structural features (Preto *et al.* 2011; Boro *et al.* 2013). The entire Latemar Platform is essentially fractured. Limited numbers of faults have been identified (Preto *et al.* 2011), but opening mode fractures or joints appear to dominate (Boro *et al.* 2013). Zones with intense fracturing (i.e. fracture corridors) have also been identified in the platform, and correspond to the large structural lineaments evident in aerial photographs and satellite images (Boro 2012). Fractures in the Latemar Platform are mainly orientated in two perpendicular sets, trending NNW–SSE and ENE–WSW. Fractures of the NNW–SSE set are generally shorter and more closely spaced than those of ENE–WSW set (Fig. 2). Boro *et al.* (2013) argued that the NNW–SSE fracture set was developed earlier, when large mechanical differences existed within the platform. The ENE–WSW fracture set was then developed at a later stage, when mechanical differences within the platform were less pronounced as a consequence of progressive lithification during burial. The fracture timing is also supported by: (i) the parallelism between the NNW–SSE set and the Ladinian volcanic dykes traversing the platform; and (ii) the abutment of ENE–WSW-trending fractures against the same dykes (Boro 2012). Both volcanic dykes and dolomite bodies are known to be Late Ladinian, roughly coeval with the deposition of the Latemar succession (Visona 1997; Carmichael *et al.* 2008).

FRACTURE DATABASE

Fracture data from the Latemar Platform were acquired through a digital acquisition technique coupled with software called DigiFract (Hardebol & Bertotti 2013). The method makes use

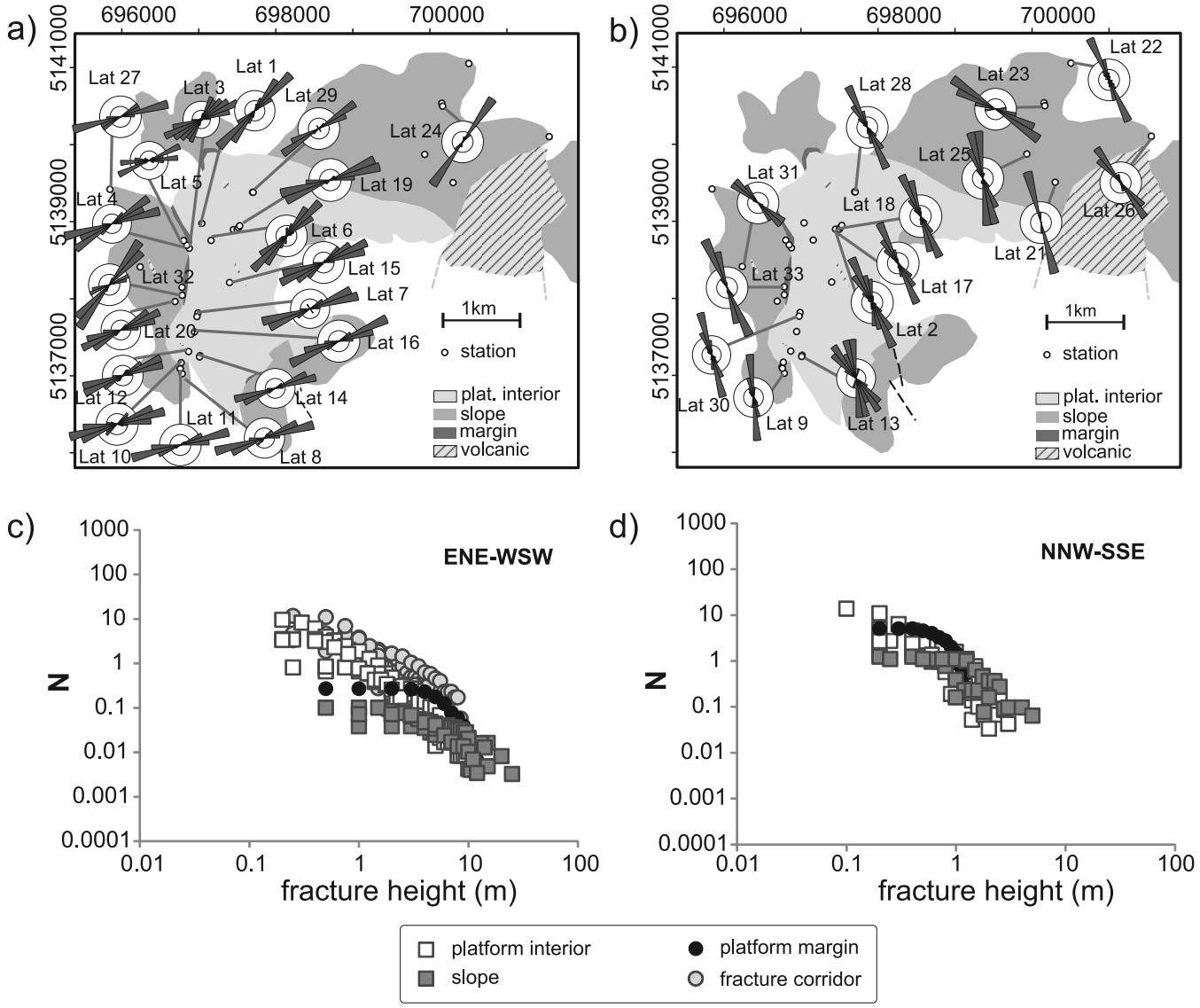

Fig. 2. Fracture characteristics in the Latemar Platform. Rose plots in (**a**) and (**b**) indicate the major fracture orientations for the ENE–WSW and NNW–SSE sets, respectively. Plots in (**c**) and (**d**) show the normalized cumulative number of fractures and the range of fracture heights measured in different sedimentological domains both for the ENE–WSW and the NNW–SSE sets, respectively. Note that fractures of the NNW–SSE set in the margin were measured on a pavement (i.e. fracture length).

of geographical information system (GIS) functionalities to capture a two-dimensional (2D) fracture distribution from the outcrops including other important geological parameters, such as layering, lithology and stiffness. Fractures were generally acquired on subvertical outcrop surfaces that enable a complete measurement of fracture size along its dip direction (i.e. fracture height). The entire dataset was then stored digitally to enable automatic calculations of fracture properties, such as fracture spacing and areal fracture intensity (P21) (Dershowitz & Einstein 1988).

The fracture database contains more than 1500 fractures collected from 33 different observation points. For representative outcrop photographs and analysis, we refer to the figures in Boro *et al.* (2013). Fractures of both NNW–SSE and ENE–WSW sets were essentially observed throughout all three distinct sedimentological domains. The strike orientations of both fracture sets typically vary within a range of 20°–30° from the mean orientations but no changes are observed from one domain to the others (Fig. 2a, b). Fractures are generally subvertical, and, in the platform interior, are generally normal to the bedding plane. The measured fracture heights in the Latemar Platform range from a few centimetres up to tens of metres (Fig. 2c, d). In the subsurface, such meso-scale fractures are rarely captured by well-bore data (e.g. Ruvo *et al.* 2003).

For the purpose of this study, only 26 representative outcrops out of a total of 33 outcrops we studied on the Latemar Platform have been taken into account for fracture modelling. The chosen outcrops span the heterogeneity in fracture patterns across distinct sedimentological domains of the Latemar Platform – slope, margin and platform interior – excluding those observed in the synsedimentary collapsed blocks (e.g. Emmerich *et al.* 2005). Owing to the limited exposure, fractures in the margin of the Latemar Platform were acquired from only two outcrops. Fracture measurements were also acquired in several fracture corridors observed in the platform, marked by high fracture intensity. The entire dataset provides an overview of the characteristics of distributed fractures in the carbonate platform body.

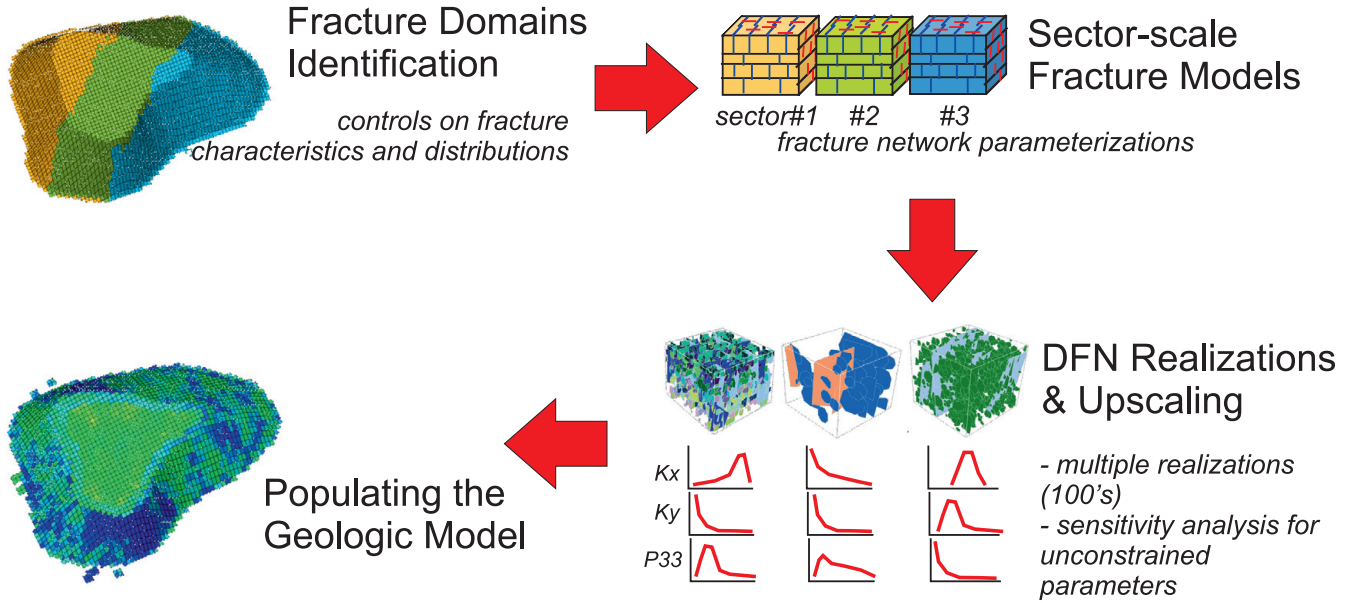

Fig. 3. General workflow for fracture modelling and upscaling.

FRACTURE MODELLING WORKFLOW AND SET-UPS

The overall workflow adopted for fracture modelling is described in Figure 3. In the first step, various statistical parameters for the fractures were cross-plotted to identify fracture domains; that is, parts of the carbonate platform characterized by fractures with similar geometrical characteristics (intensities, heights, distribution and termination patterns). In this step, factors controlling the fracture population were investigated to observe the relationships between fracture patterns and various geological parameters, such as sedimentology and bedding surfaces. Fracture models were then generated independently for each fracture domain, referred to here as sector models. Fracture characteristics derived from the statistical analysis of each domain – fracture intensity, fracture height distribution and orientations – were then used to constrain inputs for fracture-network modelling.

Fracture modelling was conducted with Fracman Reservoir Edition (FRED)^{TM} software, an application that implements a discrete fracture network (DFN) method (Dershowitz & Einstein 1988). The FRED computations include fracture model realizations and a calculation of the hydraulic properties of the fracture network. For this purpose, the areal fracture intensity (P21) values measured from the outcrops in the Latemar Platform have been transformed into volumetric fracture intensity (P32) values through a stereological method proposed by Wang (2005). The method derives the transformation factor based on the empirical relationship between fracture orientations, the angle of sampling direction and the fracture intensity (P10 or P21) (Wang 2005). As a result, there is only one solution of P32 for a given P10 or P21 value, and the transformation is generally linear (Fig. 4). This approach is different from stochastic simulation that produces a number of possible solutions for volumetric fracture intensity (P32) (e.g. Mauldon 1994; Ruvo *et al.* 2003; Casciano *et al.* 2004).

To maximize the efficiency of the computation, the vertical dimension of each model is mainly determined on the basis of the fracture heights. The resulting models are much smaller than a typical reservoir-scale model that may cover several square kilometres in area and contain hundreds of thousands of cells. With such a small volume, the computation was generally fast,

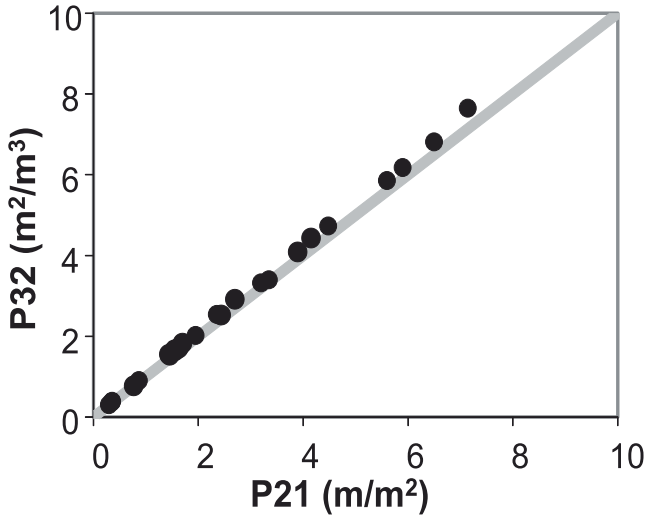

Fig. 4. P21 to P32 transformation results for fractures in the Latemar Platform through a method proposed by Wang (2005).

enabling hundreds of fracture realizations and upscaling routines. Multiple realizations are particularly important to account for various uncertainties related to the stochastic approach used to generate fracture models and various unconstrained fracture geometrical parameters such as fracture orientation, aperture and shape. In contrast, the flexibility to perform multiple realizations and upscaling at the reservoir-scale models is very limited. In addition, upscaling results based on the small-scale models could be inserted directly into the reservoir model, according to the distribution of fracture domains (Yose *et al.* 2001).

Oda's method (Oda 1985) has been implemented to estimate the effective hydraulic properties of the fractures. The method provides a robust and fast calculation based on the overall geometry of the fractures and the assigned intrinsic permeability. However, the method does not account for fracture-network connectivity. Consequently, results from the calculation could be optimistic, especially in the low fracture intensity regime where fractures are potentially less interconnected. However, we consider Oda's

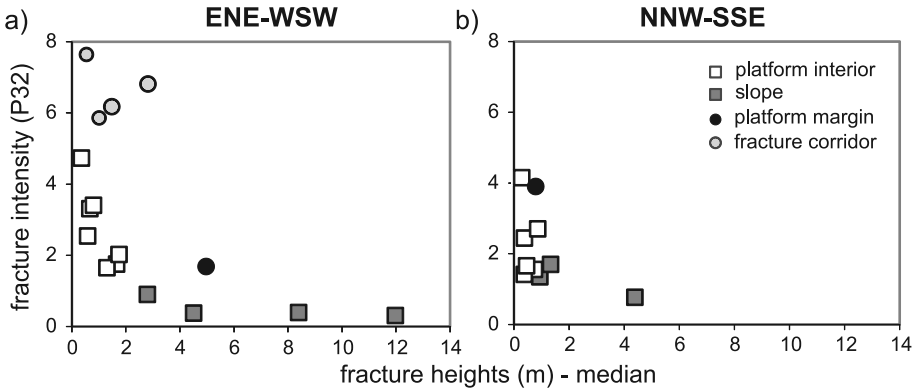

Fig. 5. Relationship between fracture height and fracture intensity (P32) in different sedimentological domains of the Latemar Platform. (**a**) ENE–WSW set. (**b**) NNW–SSE set. Note that fractures of the NNW–SSE set in the margin were measured on a pavement (i.e. fracture length).

method to be sufficient to highlight the overall modelling workflow and simulation method presented in this study.

Fracture domains in the Latemar Platform

Fracture analysis performed in the Latemar Platform (Boro *et al.* 2013) indicates that fracture characteristics are strongly affected by the first-order sedimentological properties. A cross-plot between fracture intensity (P32) and fracture heights in Figure 5 indicates a distinctive data clustering based on different sedimentological domains. Fractures in the slope domain typically have low intensities (*c.* 0.5 m^{-1}), but are taller compared to the other domains. In the platform interior, fracture intensities are notably higher (1–5 m^{-1}) and their heights are significantly shorter (<1–2 m) compared to those in the slope domain (>5 m). Fractures in the margin domain were derived only from two outcrops, but are typically taller than those in the platform interior with moderate fracture intensities (2–4 m^{-1}). In fracture corridors, fracture intensities are extremely high (>6 m^{-1}) and fractures are 1–2 m tall. The trend of the data points also suggests that fracture intensity generally decreases towards tall fractures. This is particularly evident for the ENE–WSW set (Fig. 5a), while the NNW–SSE set is less clear, perhaps due to data sampling.

More detailed investigations in the platform interior of the Latemar Platform suggest that the sedimentary layers exert only limited control on fracture patterns (Boro *et al.* 2013). Fractures are mostly distributed and confined within groups of sedimentary layers characterized by similar fracture intensity; that is, fracture units as defined by Laubach *et al.* (2009). In general, fracture spacing increases with the fracture unit thicknesses, and units that contain more grain-supported layers (grainstone–packstone) are more fractured than those that are dominated by mud-supported layers (wackestone).

In a simplified depositional model of the Latemar Platform interior (Fig. 6a), the grain content generally increases when moving from the inner lagoon towards the margin (Egenhoff *et al.* 1999). Such generalization then serves as an approximation for the distribution of fracture units of different dominant lithologies, where mud-supported fracture units are more pronounced in the deepest part of the lagoon, while grain-supported units are more dominant in the area close to the platform margin (Fig. 6b).

To apply such classifications, outcrops in the interior of the Latemar Platform were first differentiated into several facies associations: grainy facies, muddy facies and mixed facies. Outcrops that contain >50% grain-supported layers over a 10 m interval were classified as grainy facies, and vice versa for muddy facies. The mixed facies was characterized by a nearly 50:50 proportion between the grain-supported layers and the mud-supported layers. In the next step, outcrops from the same

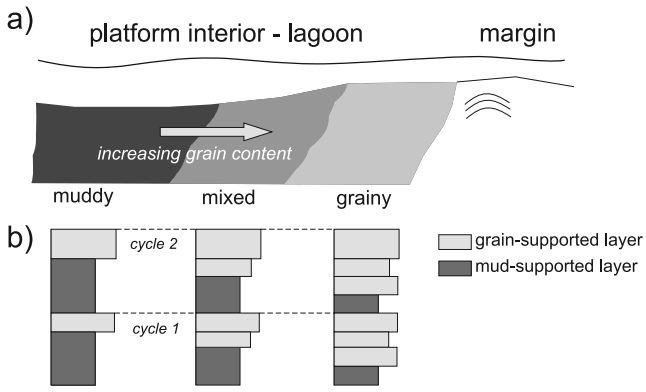

Fig. 6. (**a**) Conceptual model of facies distribution inside the platform interior (after Egenhoff *et al.* 1999). (**b**) Typical stratigraphic compositions associated with different facies.

facies were grouped together and the P32 estimation was also calculated for each fracture unit interpreted in all the outcrops inside the platform interior.

The results are shown in Figure 7. The clustering of data points is evident from the plot, especially for the ENE–WSW set. Fracture units from different facies are typically characterized by distinctive relationships between the fracture height and the fracture intensity (P32). In general, fracture units in grainy facies have higher intensities and shorter fractures compared to those of muddy facies. In the mixed facies, fracture intensities are typically low, and fracture heights vary for different sets. The results align with the general fracture termination and fracture hierarchy patterns in the Latemar Platform (Boro *et al.* 2013). The study shows that: (i) juxtapositions between grainy layers terminate more fractures than juxtapositions between muddy layers; and (ii) based on the fracture hierarchy, short fractures are distributed at narrower spacing and, therefore, higher fracture intensity than those of tall fractures. Consequently, with more terminations, fractures in the grainy facies are potentially shorter and more closely spaced than those in the muddy facies. In the case of juxtapositions of different lithologies (grainy v. muddy layers), such as those in the mixed facies, the bedding planes are less effective in terminating the fractures, therefore fractures are tall and the intensity is low.

The analysis based on different fracture sets also highlights some differences, namely that the ENE–WSW-trending fractures contain more tall fractures than those of the NNW–SSE-trending set despite the similarity in the range of fracture intensity values. The general trend of the data points indicates decreasing fracture intensity towards large fractures, consistent with the analysis from the outcrop-scale dataset in Figure 5.

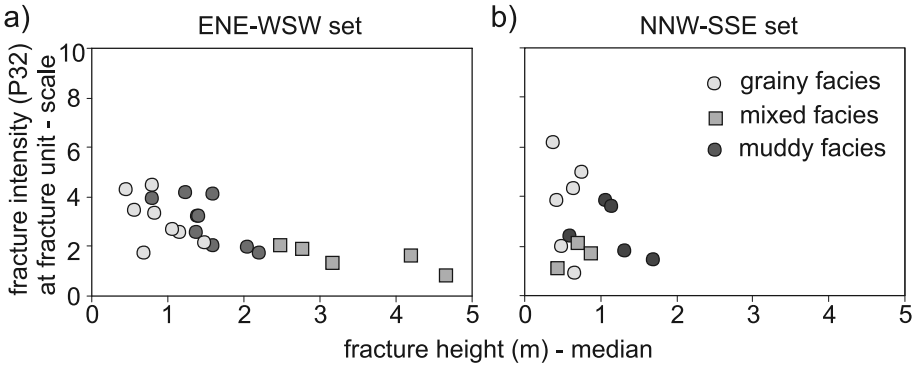

Fig. 7. The relationship between fracture height and fracture intensity (P32) for fracture units of different facies associations. (**a**) ENE–WSW set. (**b**) NNW–SSE set.

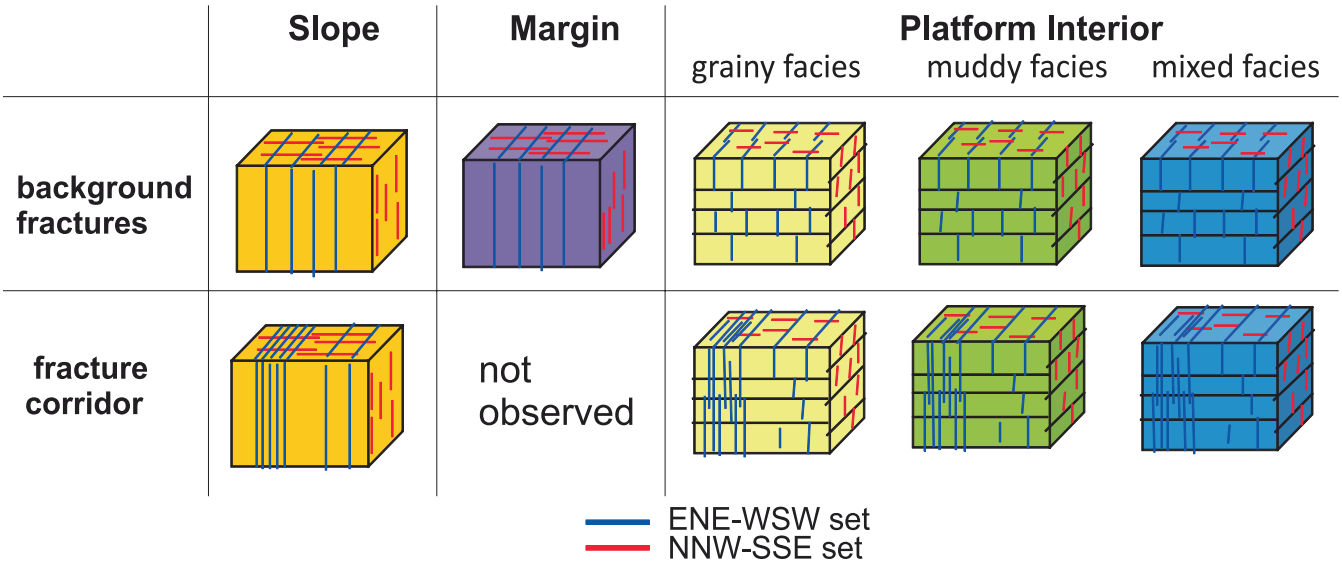

Fig. 8. Schematic models for different fracture domains in the Latemar Platform. For domains inside the platform interior – grainy, mixed and muddy facies – fractures are largely constrained within the fracture units. In the slope and margin, no stratification was included and fractures are distributed randomly. Note the presence of two different fracture sets.

The overall results clearly indicate that fracture patterns in the Latemar Platform are affected by the first-order sedimentological heterogeneities and the structural context. Based on the analysis presented above, nine different fracture domains have been assumed in the Latemar Platform (Fig. 8). In general, fracture domains are grouped based on their sedimentological composition. Background fractures and fracture corridors are also distinguished in each domain.

DFN parameterization and strategy

The maximum height of the fractures was used to define the vertical dimension of the models. Sector models for the slope and margin domains were set to 20 m high to capture the presence of fractures >15 m in height. Fractures in the platform interior are typically less than 10 m tall; thus, the height of the model was set to 10 m. The lateral dimensions (width and horizontal length) of each sector were set to 20×20 m to optimize the computational process. It is important to note that the lateral dimension of the sector model should be adjusted according to the cell size in the reservoir model to allow a direct implementation in distributing the hydraulic properties of the fractures.

Values for different input parameters are given in Figure 9 and are referred to here as the base case scenario. The statistical characteristics of fracture networks for each fracture domain – namely, the fracture intensity, radii and orientations – were extracted from the results of outcrop analysis. For modelling, the range of fracture radii in the model was estimated based on the fracture height distribution from the outcrop measurements. The orientations of the fractures (strike and dip) measured in the Latemar Platform have been normalized against the regional bedding dip.

For sector models in the platform interior (grainy, muddy and mixed facies), stratification was included to model the fractures that are confined within fracture units as observed in the outcrops. For the base case scenario, the thickness of the fracture units is uniform and was constructed based on the average fracture unit thickness observed in each domain. Fractures that are taller than the fracture unit thickness were populated randomly in the model with a lower intensity. No stratification was included in the slope and margin domains, as the sediments are massive and fractures are distributed randomly within each domain. For the purpose of modelling, the *x*-axis of the fracture model was set parallel to the mean orientation of the ENE–WSW fractures, while the NNW–SSE set was set parallel to the *y*-axis. Cross-cutting relationships between these two sets were defined according to their relative age as postulated by Boro *et al.* (2013).

Fracture intensities measured in the outcrops of the Latemar Platform are generally higher than those reported in subsurface carbonate reservoirs (<1 m^{-1}) (e.g. Ruvo *et al.* 2003; Narr *et al.* 2008; Laubach *et al.* 2009). For this study, we adopted a fracture

				Background Fractures					Fracture Corridors			
				Slope	Margin	Grainy	Mixed	Muddy	Slope	Grainy	Mixed	Muddy
model dimension (WxLxH) (m)				20x20x20		20x20x10			20x20x20	20x20x10		
ENE-WSW set (trend=180, plunge=05)	generation model			Enhanced Beacher					Levy Lee (1 step, fractal dimension=10)			
	dispersion coefficient (k)			80					200			
	confined fractures	***Fracture Unit Thickness***		NA		1	3.5	1.5	NA			
		P32				0.35	0.15	0.3				
		fracture radii (m)	distribution			lognormal						
			mean			1.1	3.5	1.6				
			deviation			0.35	0.35	0.35				
	through-going fractures	P32		0.03	0.2	0.15			0.65			
		fracture radii (m)	distribution	lognormal					lognormal			
			mean	10	5	3			5			
			deviation	3.5	2.5	1.5			3.5			
	shape ratio			1:1					1:1			
	number of side			8					8			
	aperture (a)			Normal (mean=0.005,dev=0.005)					Normal (mean=0.005,dev=0.005)			
NNW-SSE set (trend=90, plunge=05)	generation model			Enhanced Beacher					Enhanced Beacher			
	dispersion coefficient (k)			60	130	80			60	80		
	confined fractures	***Fracture Unit Thickness***		NA		1.5	1	1	NA	1.5	1	1
		P32				0.35	0.15	0.25		0.35	0.15	0.25
		fracture radii (m)	distribution			lognormal				lognormal		
			mean			0.6	0.75	1.2		0.6	0.75	1.2
			deviation			0.35	0.35	0.45		0.35	0.35	0.45
	through-going fractures	P32		0.15	0.4	0.15			0.15			
		fracture radii (m)	distribution	lognormal					lognormal			
			mean	2.5	0.8	3			2.5	3		
			deviation	1.5	0.4	1.5			1.5	1.5		
	shape ratio			1:1					1:1			
	number of side			8					8			
	aperture (a)			Exponential (e=0.0001)					Exponential (e=0.0001)			

Fig. 9. DFN input parameters for all fracture domains in the base case scenario. Parameters with bold letters are subjected to sensitivity analysis. Input values are mainly derived from outcrop measurements (i.e. fracture orientation and dispersion coefficient (*k*), fracture intensity, and fracture unit thicknesses). Measurements of fracture heights have been used as inputs for fracture size characteristics, the fracture radii. Other parameters (i.e. fracture generation algorithm, fracture shape and fracture-aperture statistics) are conceptual.

intensity that is 10% of the actual fracture intensity value in all fracture domains and fracture units (Fig. 9), resulting in P32 values comparable with the subsurface observations. No aperture values have been measured from the outcrops in the Latemar Platform due to intense weathering that might have influenced the present-day fracture-aperture value. In this study, a conceptual aperture setting has been applied in which we assumed that the ENE–WSW set contains more open fractures than those of the NNW–SSE set. In the model, the aperture values for the ENE–WSW fracture set follow a normal distribution that ranges between 0 and 1 mm, with an average aperture of 0.5 mm. For the NNW–SSE fracture set, the range of aperture values follows a negative exponential distribution for up to 0.5 mm.

During the realizations, the intrinsic permeability of each fracture was estimated by adopting a 'cubic-law' approximation according to which the permeability of each fracture is calculated on the basis of the fracture-aperture value (e.g. Whiterspoon *et al.* 1980; Agar *et al.* 2010). Multiple realizations were then conducted for each sector model by adopting Oda's method to calculate the effective fracture permeability and fracture porosity (Oda 1985). Each sector model consists of only one grid cell. Therefore, the calculation results derived from each fracture model could represent the hydraulic properties of fractures within one particular grid cell of the reservoir model. The results from each sector domain were then grouped and compared with each other to infer the impact of fracture-network characteristics on fluid flow.

Sensitivity analysis was also conducted to investigate the impacts of unconstrained parameters on the upscaled hydraulic properties. For this purpose, we focused on the variation of fracture unit thicknesses as observed in the outcrops: the fracture shape (height:length ratio), the dispersion of fracture orientations and the fracture-aperture setting. In total, we have upscaled 4200 different fracture models, covering different fracture domains and various sensitivity analyses (100 realizations for each domain and for each scenario). Application of such an extensive multi-realization technique in capturing uncertainties related to fracture-network characteristics is clearly limited in the conventional full-field modelling approach.

RESULTS: FRACTURE-NETWORK ANALYSIS

Base case scenario

The upscaling results from the base case scenario are given in Figure 10. In general, the effective permeability and porosity of

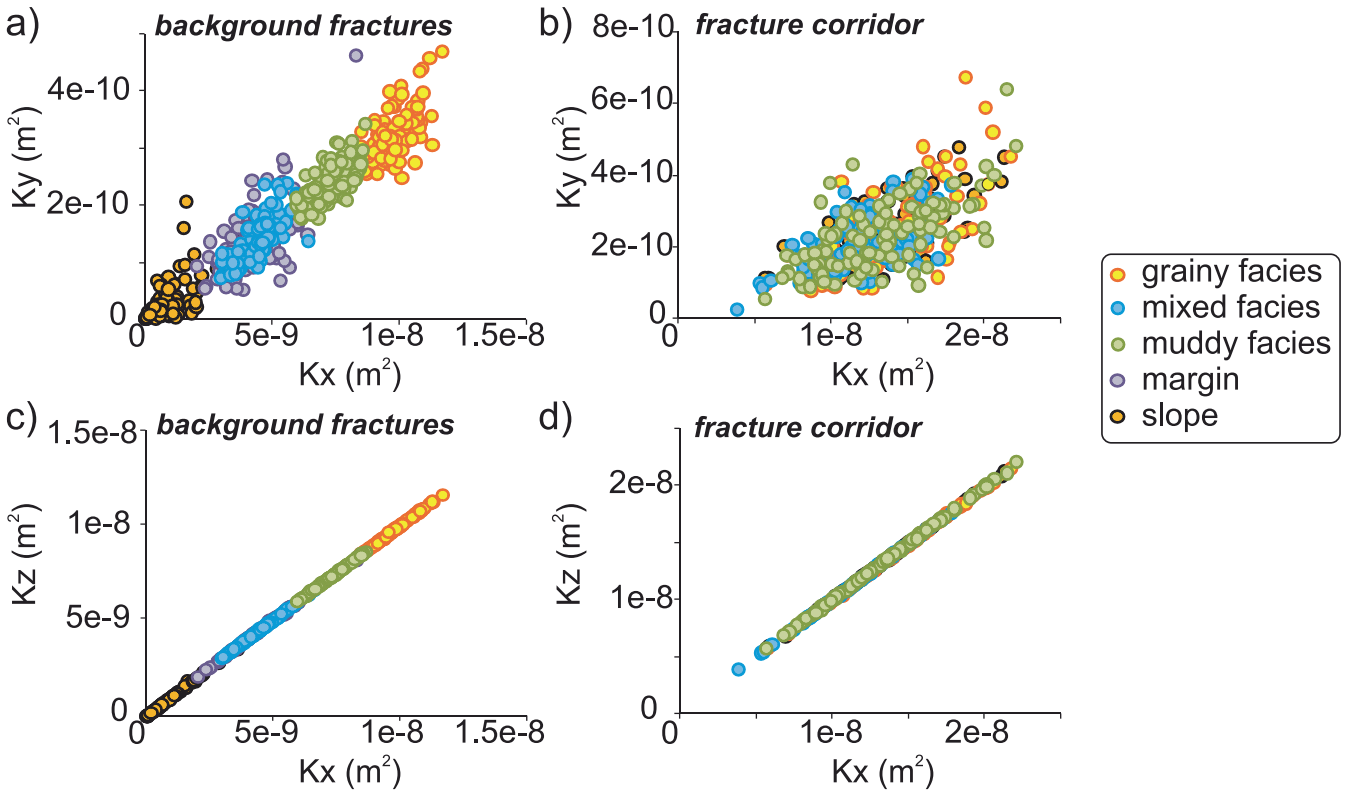

Fig. 10. Upscaling results for different fracture domains of the Latemar Platform. Effective fracture permeability in horizontal axes (K_x and K_y): (**a**) for the background fractures; and (**b**) for the fracture corridors. Relationships between effective fracture permeability in the vertical axis (K_z) and in the horizontal *x*-axis (K_x): (**c**) for background fractures; and (**d**) for the fracture corridors. Note that in the model, the *x*-axis is parallel to the ENE–WSW fracture set and the *y*-axis is parallel to the NNW–SSE fracture set.

the fractures vary for different sedimentological domains, underlining the role of changes in fracture-network characteristics in influencing fluid flow across different parts of the reservoir.

Effective fracture permeability values for domains inside the platform interior (grainy, muddy and mixed facies) are significantly higher than those in the slope and margin (Fig. 10a). Fractures in grainy facies account for the highest effective fracture permeabilities in horizontal directions, $>10^{-8}\,m^2$ (equivalent to $>10^6$ mD) along the ENE–WSW set (*x*-axis), and $>3\times10^{-10}\,m^2$ (equivalent to $>3\times10^4$ mD) for the NNW–SSE set (*y*-axis). The effective fracture permeability in the horizontal plane decreases gradually from muddy to mixed facies. The slope domain accounts for the lowest effective fracture permeabilities along both the ENE–WSW set (*x*-axis) and the NNW–SSE set (*y*-axis). Despite the differences in fracture-network characteristics, the effective fracture permeabilities in the margin extend over a range similar to those in the platform interior, especially for mixed facies.

Results from fracture corridors are significantly different (Fig. 10b, d). Effective fracture permeability values are considerably higher than those of the background fractures and show no differentiation through different sedimentological domains. In general, the effective fracture permeabilities parallel to ENE–WSW-striking corridors (*x*-axis) are more than twice as high as those of the NNW–SSE set (*y*-axis). In the slope, the effective fracture permeability of a fracture corridor is up to three orders of magnitude higher than the background fractures. A similar trend is also valid for the effective permeabilities in the vertical axis (K_z) but at different magnitudes (Fig. 10c).

The upscaled permeability results indicate an anisotropic permeability field with a strong preferential direction for flow. From the upscaling results, effective fracture permeability parallel to the ENE–WSW set (*x*-axis) is typically more than two orders of magnitude higher than that of the NNW–SSE set (*y*-axis). Such a pattern is observed for both background fractures and fracture corridors (Fig. 10a, b). The effective fracture permeabilities in the vertical direction (K_z) are similar to those in the horizontal direction along the *x*-axis (Fig. 10c, d). Figure 11 shows, schematically, the fracture permeability field throughout different domains. The general orientations of the permeability tensor are constant, but their magnitude decreases when moving from the muddy part of the platform interior towards the slope domain.

The impacts of different fracture-network characteristics are also evident from the effective fracture porosity (P33) (Fig. 12). Fracture networks in the grainy facies have the highest effective porosities, while the slope accounts for the lowest values (Fig. 12a). The effective porosity is linearly related to the effective permeability in the horizontal direction along the ENE–WSW set (*x*-axis) (Fig. 12b). Such behaviour is mainly related to the applied fracture-aperture setting, in which the ENE–WSW fracture set contains more open fractures with wide aperture.

It is important to note that the calculation results from the margin domain are associated with a large uncertainty owing to limited data. Statistical analysis from only two outcrops clearly prevents detailed characterizations of the actual range of fracture intensities and fracture heights. With more observations, the hydraulic properties of the fractures in the margin domain might shift considerably.

Sensitivity analysis

Several DFN parameters in the base case scenario are not well constrained from outcrop analysis. In our sensitivity analysis, we focused on the impacts of thickness variations of fracture units,

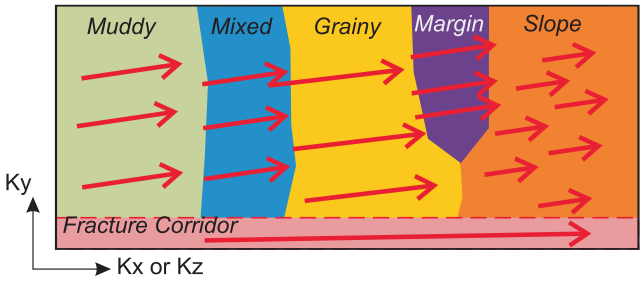

Fig. 11. Schematic fracture permeability field across different domains of the Latemar Platform.

different fracture shape ratio, dispersion level of the fracture orientations and fracture-aperture set-ups on the upscaled hydraulic properties of the fracture network. Figure 13 highlights the main differences in the modelling set-ups between the base case scenario and the sensitivity analysis.

To improve comparisons of results from the sensitivity analysis, we calculated a parameter C (equation 1), defined here as the ratio between the results from sensitivity analysis (A') over the base case scenario (A):

$$C = \frac{A(\text{median})}{A(\text{median})}. \quad (1)$$

The ratio was then calculated for both the effective permeability tensor (K_x, K_y, K_z) and the effective porosity (P33) in different fracture domains. From 100 model realizations, the median value of permeability tensor and porosity was chosen to represent the results from each case in the sensitivity analysis, including the base case scenario. Figure 14 shows the comparison between the overall results from the sensitivity analysis and the base case scenario.

Variation in fracture unit thicknesses. In the Latemar Platform, the thickness of fracture units ranges from tens of centimetres up to a few metres (Boro *et al.* 2013). In the base case scenario, the average fracture-unit thickness was adopted to construct the model. Consequently, fracture models for domains in the platform interior contain a uniform thickness of fracture units with similar statistical characteristics for fracture radii and fracture intensity (P32). In our sensitivity analysis, two different thicknesses of fracture units have been applied to capture the minimum and the maximum fracture heights separately in the model, as highlighted in Figure 7. With this set-up, the radii and the intensity of the fractures vary vertically according to the thickness of the fracture unit (Fig. 13a).

The upscaling results from the model with various fracture unit thicknesses indicate C values that are close to 1, implying that the effective fracture permeabilities and porosity results are similar to those of the base case scenario (Fig. 14a). The results suggest that the upscaled results are not really sensitive to the detailed positions and arrangement of the fractures within the model. Applying average fracture intensity (P32) and fracture radii is, therefore, considered sufficient in upscaling the hydraulic properties of the fractures.

The role of fracture shape. As our measurements in the Latemar have been performed mainly on the 2D vertical surfaces of outcrops, information on fracture lengths is generally absent, preventing a detailed characterization of the 3D fracture geometry. In the base case scenario, fracture height measurements from the outcrop have been used to estimate the fracture radii in the model, while the fracture-shape ratio was assumed to be 1:1 (Fig. 13b). For the sensitivity analysis, we explore the effect of changing the shape ratio to 1:5 (the length of the fractures is five times their heights) on the upscaling results. The fracture radii statistical set-up was kept equal to the base case scenario.

The results from effective property calculations indicate only small differences with those from the base case scenario (Fig. 14b). Similar to the fracture-unit thickness test, the C values are typically close to 1 for all of the hydraulic parameters in different fracture domains. This result indicates that the shape of the fractures is of minor importance in the upscaling process, especially when the overall statistical characteristics of the fracture radius and fracture intensity are well constrained.

Variation in the dispersion level of fracture orientation. In the base case scenario we assumed a relatively low dispersion of fracture strikes in all domains of the platform; that is, fractures of each set are well aligned. For the sensitivity analysis, a higher dispersion level was applied to both sets. For this purpose, the dispersion coefficient (k) values were set to be half of those used in the base case scenario in all fracture domains (Fig. 13c).

The effective permeability and porosity results that were computed with a higher dispersion level, however, do not show significant differences from the base case scenario (Fig. 14c). The C parameter indicates values that are nearly equal to 1, with only minor differences in some domains. This result indicates that the dispersion level of the fracture orientation also has little influence on effective permeability and porosity estimations for the scenarios that we are evaluating.

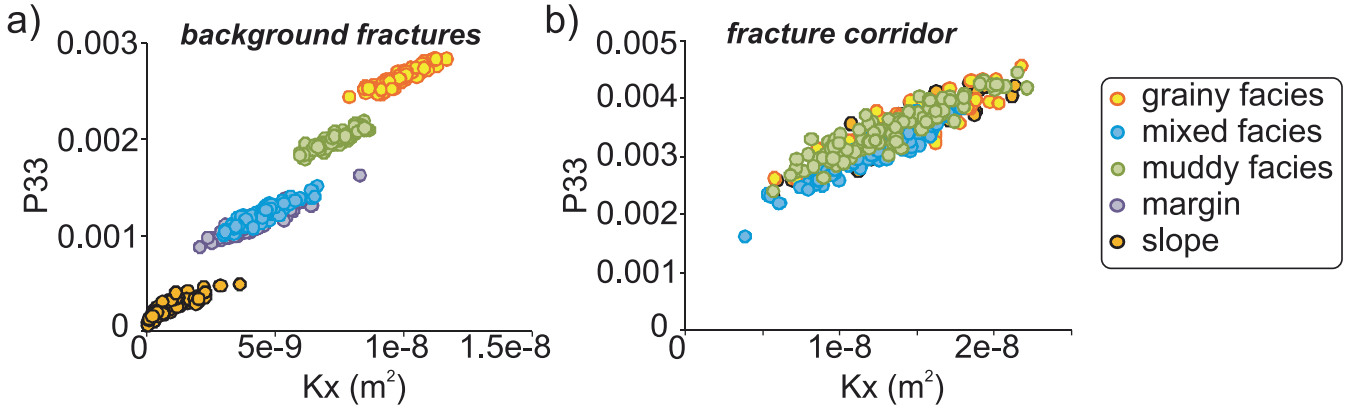

Fig. 12. The relationship between the horizontal permeability (K_x) and the effective fracture porosity (P33): (**a**) for background fractures; and (**b**) for fracture corridors.

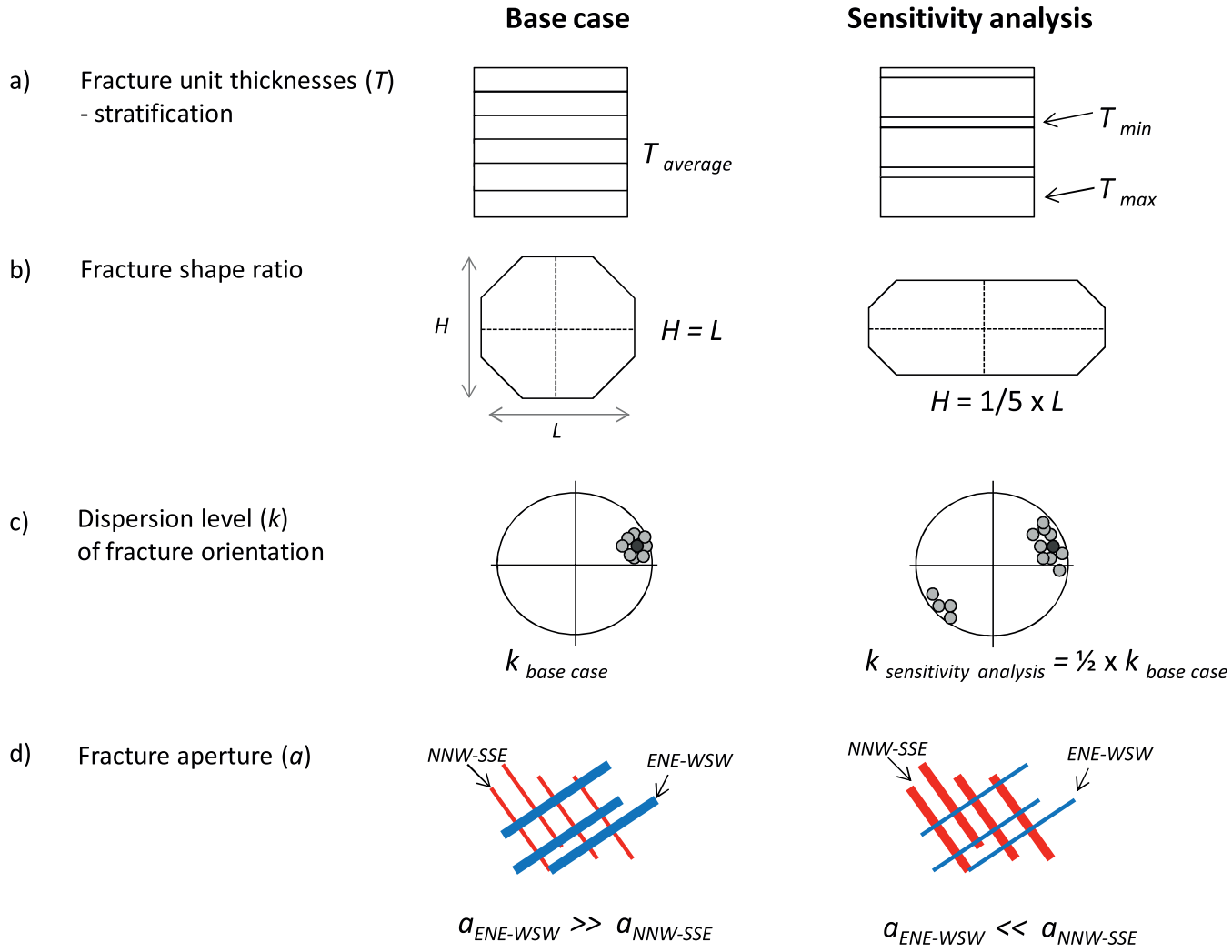

Fig. 13. Comparisons between the fracture modelling set-ups applied in the base case scenario and in the sensitivity analysis. (**a**) Fracture unit thicknesses (*T*). Note the differences in the stratification scheme of both cases. (**b**) Fracture shape ratio (*H*, fracture height; *L*, fracture length). Fractures were modelled with eight-sided geometry. Note that, in the DFN approach, the surface area of fractures in both cases is equal, calculated based on the fracture radii input. (**c**) Schematic stereoplots showing differences in the dispersion level (*k*) of fracture orientations in both cases. Dark grey dots in the plots indicate the mean fracture orientation. (**d**) Variation in fracture-aperture (*a*) set-ups applied for different fracture sets.

Changes in fracture-aperture values. Many studies have documented the role of fracture aperture in affecting fluid flow (e.g. Philip *et al.* 2005; Klimczak *et al.* 2010). In sensitivity analysis, the aperture settings adopted for the two sets in the base case scenario were exchanged. As a result, the NNW–SSE set (parallel to the *y*-axis) contains more open fractures and larger aperture values than those of the ENE–WSW trending set (parallel to the *x*-axis) (Fig. 13d).

The upscaled results from the new aperture set-up are significantly different (Fig. 14d). The effective fracture permeabilities in the direction of the ENE–WSW set (*x*-axis) decreased by more than one order of magnitude with respect to the base case scenario, except in the slope where the differences in effective fracture permeabilities are less pronounced. For fractures in the NNW–SSE set (*y*-axis), the effective permeabilities generally increased by more than one order of magnitude. The vertical effective fracture permeability (K_z) and fracture porosity (P33), however, only show small changes over the base case scenario.

Differences in the upscaling results are largely due to the 'cubic-law' implementation of the intrinsic fracture permeability. Therefore, for subsurface reservoirs, a more detailed analysis is required to determine the appropriate intrinsic permeability based on laboratory measurements on core samples. The overall results also highlight the need to investigate the main factors that govern fracture apertures, their characteristics and their distributions (Bertels *et al.* 2001; Klimczak *et al.* 2010).

Fracture cluster and inference on reservoir connectivity

In fractured reservoirs, interconnected fractures or fracture clusters play an important role in affecting reservoir productivity (Moinfar *et al.* 2011). In general, interconnected open fractures provide efficient pathways that will improve hydrocarbon extraction. However, an extensive interconnected fracture system could also trigger early water-breakthrough or production interference between wells that limit the reservoir productivity (Namba & Hiraoka 1995). Consequently, quantifying and understanding the fracture connectivity is one of the key aspects in developing fractured reservoirs (Makel 2007). In general, the extent of interconnected fractures is strongly affected by fracture intensity, orientation, the number of sets and fracture geometry (e.g. Balberg *et al.* 1991; Gillespie *et al.* 1993; Odling *et al.* 1999; Ghosh & Mitra 2009).

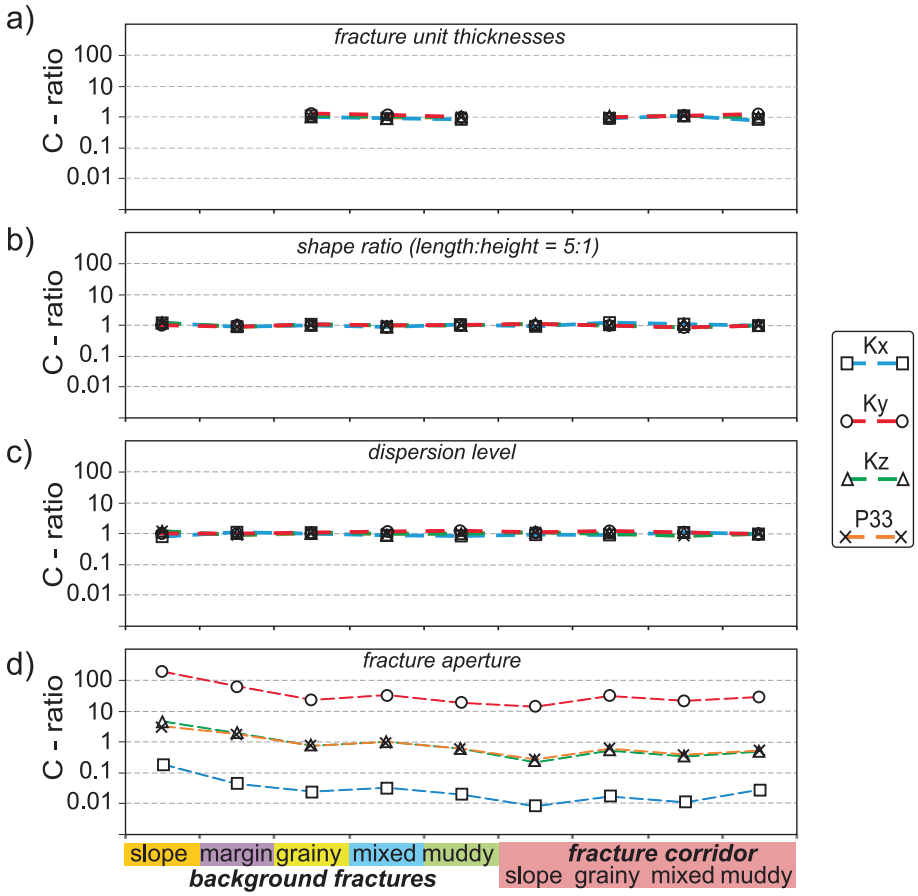

Fig. 14. Upscaled results for the cases in sensitivity analysis: (**a**) variation in the fracture unit thicknesses; (**b**) changes in the fracture shape ratio; (**c**) different dispersion level of fracture orientation; and (**d**) different fracture-aperture set-up. Comparison with the base case scenario is indicated by the *C* ratio values, calculated based on the median value of fracture's effective permeability tensor (K_x, K_y, K_z) and fracture porosity (P33) in different fracture domains (indicated by lines of different line patterns).

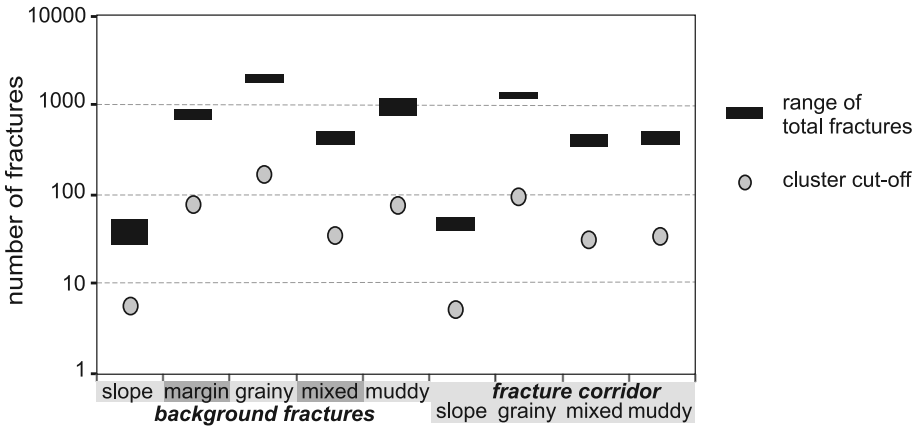

Fig. 15. A plot showing the range of total fractures contained in each sector model after all DFN simulations (black boxes). Grey dots indicate the minimum amount of interconnected fractures within a fracture cluster.

In this study, we analysed the extent of fracture clusters as a result of variations in fracture-network characteristics across domains in the Latemar Platform. Different cut-off values defining a fracture cluster were set independently for each domain to account for differences in fracture intensity and fracture heights (Fig. 15). For the analysis, a cluster was defined as a zone in which more than 10% of the fractures in the model are interconnected. The chosen cut-off value was assumed to have a sufficient number of interconnected fractures that would contribute to fluid flow. In the slope, for instance, a cluster consists of around 10 interconnected fractures due to large fracture radii, while more than 100 interconnected fractures are required in grainy facies due to their small radii.

In each realization, the volume occupied by a fracture cluster was calculated relative to the overall volume of the model (as a percentage). The results serve as a proxy to the extent of interconnected fractures and connectivity. A high percentage value indicates extensive interconnected fractures throughout the model and, therefore, good reservoir grid connectivity in all directions (horizontal and vertical). In contrast, a low percentage suggests localized interconnected fractures and relatively poor connectivity in the reservoir grid.

Figure 16 summarizes the overall results of the fracture cluster analysis. In the base case scenario (thick grey line in Fig. 16), interconnected fractures occupy only about 55% of the model volume, therefore the connectivity is relatively poor. This is true for the majority of domains, except for the muddiest part of the platform interior. A high fracture intensity of large fractures in the muddy facies clearly has contributed to an excellent connectivity between fractures where the cluster volume occupied up to

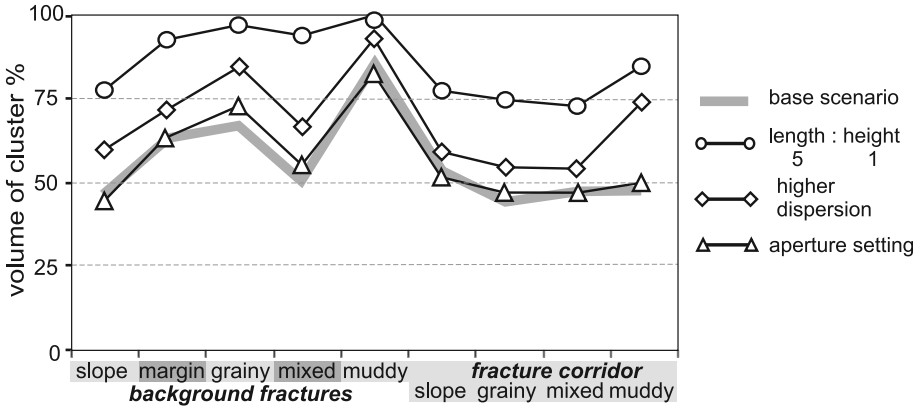

Fig. 16. Volume of clustered fractures for fracture models of different domains, and for various sensitivity scenarios. The volume of the clustered fractures serves as a proxy to the extent of interconnected fractures.

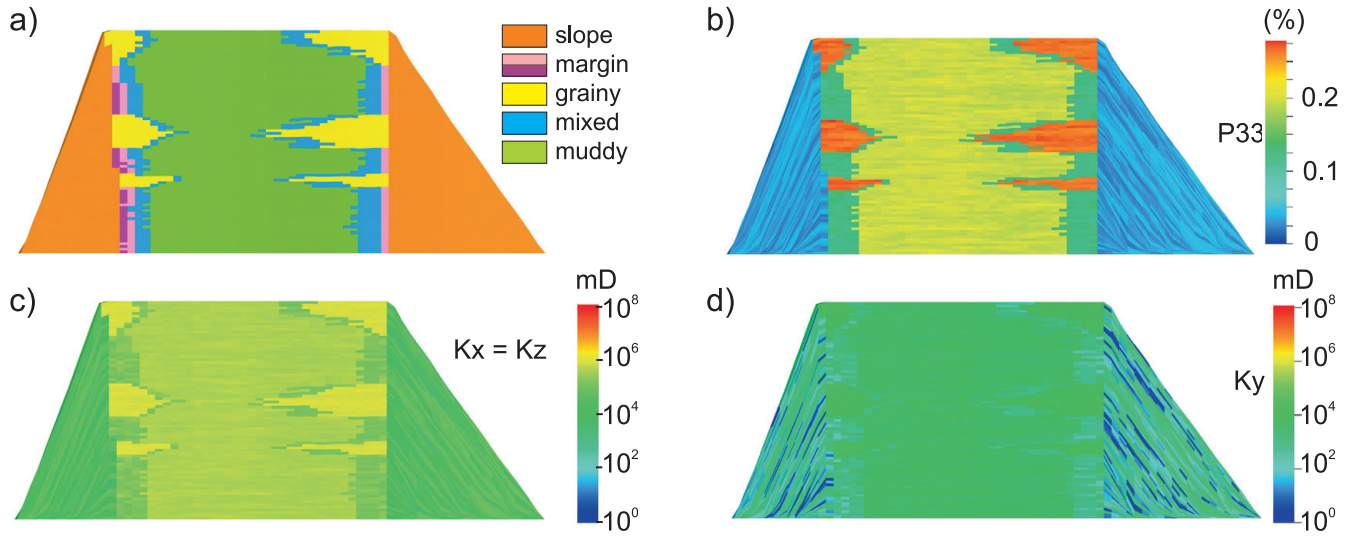

Fig. 17 Conceptual reservoir model of the Latemar Platform. (**a**) Facies model. (**b**) Fracture porosity (P33) distribution. Plots (**c**) and (**d**) are for the permeability tensor (K_x, K_y, K_z).

85% of the volume. In the slope domain, the combination of large fractures and low fracture intensity results in much smaller fracture cluster volumes, and, therefore, poorer connectivity. In fracture corridors, the volume of the clusters is small, similar to those observed in the slope. This behaviour is expected, as the fractures inside the corridors are typically concentrated only in a narrow zone.

The sensitivity analysis over various DFN parameters also provides insights into the role of fracture characteristics on connectivity. Differences in fracture-aperture patterns for different sets do not generate significant changes in the cluster size (line with triangle markings in Fig. 16). In general, volumes of the clustered fractures in different domains are similar to those of the base case scenario. A significant increase in cluster volume is observed when the shape ratio of the fractures becomes 1:5 (fracture lengths are five times their heights: line with circle markings in Fig. 16). The results point to an increase of >20% in the volume of fracture clusters in all of the fracture domains. Such results clearly underline the role of fracture shape in affecting the connectivity between fractures, and between reservoir grids.

The results from the higher dispersion level also show a significant increase in the volume of interconnected fractures (line with diamond markings in Fig. 16), around 10–15% above the base case scenario. In fracture corridors, for instance, the volume of interconnected fractures has increased by >5% from the base case scenario. Such a result shows that highly dispersed fracture orientations will enhance the fracture connectivity and, therefore, improve the grid-cell connectivity.

FRACTURE PROPERTIES IN RESERVOIR MODELS

As discussed above, the analysis of the upscaled hydraulic properties from various sector models provides a general overview of the fluid flow across different parts of the reservoir. More accurate predictions are generally acquired through fluid flow simulations that account for the dual-porosity, dual-permeability of the system. In field development programs, fluid flow simulation is particularly useful for history matching and to estimate the overall reservoir productivity (e.g. Portella & Prais 1999; Subbey *et al.* 2002).

Using our approach, results from various sector models could be used directly to assign the hydraulic properties of the fractures for all the cells in the reservoir grid. In this case, a prior understanding of the distribution of fracture domains in the reservoir is necessary. In the case of the Latemar Platform, for instance, the sedimentological facies model could be used as the geological driver to populate the model with fracture properties as these are strongly influenced by the sedimentology (Fig. 17). For fracture corridors, structural interpretations from seismic or well data could provide a robust constraint in the model.

Reservoir characterization in naturally fractured systems is clearly challenging and potentially associated with large uncertainty. However, in the conventional static modelling approach, quantifying the uncertainty related to a fracture network is completely separated from the static model itself. With the modelling workflow presented in this study, uncertainty analysis over various fracture parameters could be easily performed and integrated as alternative scenarios related to fracture-network characteristics. Their impacts on the reservoir productivity can also be explored through dual-porosity–dual-permeability simulations.

CONCLUSIONS

The analysis in this paper has clearly underlined the strength of the adopted workflow in fracture modelling and upscaling. The efficiency of the small-scale fracture model enables multiple fracture realizations and upscaling that are important to account for various uncertainties in the fracture-network characteristics. Through the sensitivity analysis, the optimum upscaling results can be obtained and used as inputs in a dual-porosity–dual-permeability reservoir-scale model. In addition, the overall workflow is also flexible enough to incorporate different upscaling techniques. In this particular case, a flow-based upscaling technique could be easily integrated to calibrate the upscaled results from Oda's method (Oda 1985).

The integration of the outcrop observations clearly provides a deeper insight into the heterogeneity in the fracture characteristics of subsurface reservoirs. In the Latemar Platform analogue, sedimentology and diagenesis are the main controls affecting the fracture intensity, geometry and distribution. Acquiring such detailed information on the controlling factors of fracture populations could be challenging in the subsurface, especially owing to limited observations. Fractures in the outcrop might have been affected by near-surface processes such as weathering and stress release. However, the results are still useful to develop additional scenarios of fracture populations for subsurface reservoirs.

Our study demonstrates the importance of fracture networks in affecting fluid flow inside heterogeneous systems such as isolated carbonate platforms. In the case of the Latemar Platform, fracture characteristics change between sedimentological domains and also vary with different fracture sets. The results predict substantial variations in the permeability field across the platform domains and imply different flow paths. The slope domain in the Latemar Platform accounts for the lowest effective permeability due to low fracture intensity combined with large fracture radii. In contrast, the high fracture intensity of small fractures in the platform interior results in a higher effective permeability. A similar impact is also valid for the fracture-aperture values. Changes in the permeability field over two orders of magnitude are evident from the calculations. Such significant variation is partly related to the intrinsic permeability assigned to the fractures.

Other fracture parameters (fracture unit arrangement, fracture shape and orientations), however, have less influence in determining the hydraulic properties of the fractures. Their impact is more pronounced in affecting the fracture connectivity, which influences the overall grid-block connectivity within the reservoir model. Such behaviour is particularly evident from the fracture-network analysis in the platform interior. While the fracture intensity is relatively similar for both grainy and muddy facies, the resulting connectivity in muddy facies is significantly better because the fractures have larger radii than those in the grainy facies. The analysis indicates an increase of >10% in the volume of fracture clusters due to changes in the fracture shape ratio and dispersion level.

This work was carried out during the internship that the first author had at ExxonMobil URC as part of the research collaboration within the framework of 'Fundamental Controls on Flow in Carbonates – $(FC)^2$ Alliance'. Golder Associate Inc. is thanked for the use of Fracman Reservoir Edition (FRED) academic license. The content of this paper has been greatly improved by the constructive comments of the two anonymous reviewers.

REFERENCES

Agar, S., Geiger, S., Matthai, S. *et al.* 2010. The impact of hierarchical fracture networks on flow partitioning in carbonate reservoirs: Example based on a Jurassic carbonate ramp analogue from the High Atlas, Morocco. Paper SPE 135135, presented at the SPE Annual Technical Conference and Exhibition, 19–22 September 2010, Florence, Italy.

Antonellini, M. & Aydin, A. 1995. Effect of faulting on fluid flow in porous sandstones: Geometry and spatial distribution. *American Association of Petroleum Geologists Bulletin*, **79**, 642–671.

Balberg, I., Berkowitz, B. & Drachsler, G. 1991. Application of a percolation model to flow in fractured hard rocks. *Journal of Geophysical Research*, **96**, 10,015–10,021.

Bennett, R., Li, H., Lambert, D. *et al.* 1990. *In situ* porosity and permeability of selected carbonate sediment: Great Bahama Bank. Part 1: Measurements. *Marine Georesources and Geotechnology*, **9**, 1–28.

Bertels, S.P., Dicarlo, D.A. & Blunt, J. 2001. Measurement of aperture distribution, capillary pressure, relateive permeability, and *in situ* saturation in a rock fracture using computed tomography scanning. *Water Resources Research*, **37**, 649–662.

Billi, A., Salvini, F. & Storti, F. 2003. The damage zone–fault core transition in carbonate rocks: implications for fault growth, structural and permeability. *Journal of Structural Geology*, **25**, 1779–1794.

Boro, H. 2012. *Fracturing, physical properties and flow patterns in isolated carbonate platforms: A field and numerical studies of the Latemar platform (Dolomites, N Italy)*. PhD thesis, VU University Amsterdam.

Boro, H., Bertotti, G. & Hardebol, N. 2013. Distributed fracturing affecting isolated carbonate platforms, the Latemar platform natural laboratory (Dolomites, N Italy). *Marine and Petroleum Geology*, **40**, 69–84.

Bosellini, A. 1984. Progradation geometries of carbonate platforms: Examples from the Triassic of the Dolomites, northern Italy. *Sedimentology*, **31**, 1–24.

Cappa, F., Guglielmi, Y., Fénart, P., Merrien-Soukatchoff, V. & Thoraval, A. 2005. Hydromechanical interactions in a fractured carbonate reservoir inferred from hydraulic and mechanical measurements. *International Journal of Rock Mechanics and Mining Sciences*, **42**, 287–306.

Carmichael, S., Ferry, J. & McDonough, W. 2008. Formation of replacement dolomite in the Latemar carbonate buildup, Dolomites, northern Italy: Part 1. Field relations, mineralogy, and geochemistry. *American Journal of Science*, **308**, 851–884.

Casciano, C., Ruvo, L., Volpi, B. & Masserano, F. 2004. Well test simulation through Discrete Fracture Network modeling in a fractured carbonate reservoir. *Petroleum Geoscience*, **10**, 331–342.

Cooke, M. & Underwood, C. 2001. Fracture termination and step-over at bedding interfaces due to frictional slip and interface opening. *Journal of Structural Geology*, **23**, 223–238.

De Keijzer, M., Hillgartner, H., Al Dhahab, S. & Rawnsley, K. 2007. A surface–subsurface study of reservoir-scale fracture heterogeneities in Cretaceous carbonates, North Oman. *In*: Lonergan, L., Jolly, R.J.H., Rawnsley, K. & Sanderson, D.J. (eds) *Fractured Reservoirs*. Geological Society, London, Special Publications, **270**, 227–244.

Dershowitz, W. & Einstein, H. 1988. Characterizing rock joint geometry with joint system models. *Rock Mechanics and Rock Engineering*, **21**, 21–51.

Egenhoff, S., Peterhänsel, A., Bechstädt, T., Zühlke, R. & Grötsch, J. 1999. Facies architecture of an isolated carbonate platform: Tracing the cycles of the Latemar (Middle Triassic, northern Italy). *Sedimentology*, **46**, 893–912.

Emmerich, A., Glasmacher, U., Bauer, F., Bechstädt, T. & Zühlke, R. 2005. Meso-/Cenozoic basin and carbonate platform development in the SW-Dolomites unraveled by basin modeling and apatite FT analysis: Rosengarten and Latemar (Northern Italy). *Sedimentary Geology*, **175**, 415–438.

Fisher, Q. & Knipe, R. 2001. The permeability of faults within siliciclastic petroleum reservoirs of the North Sea and Norwegian Continental Shelf. *Marine and Petroleum Geology*, **18**, 1063–1081.

Ghosh, K. & Mitra, S. 2009. Two-dimensional simulation of controls of fracture parameters on fracture connectivity. *American Association of Petroleum Geologists Bulletin*, **93**, 1517–1533.

Gillespie, P., Howard, C., Walsh, J. & Watterson, J. 1993. Measurement and characterisation of spatial distributions of fractures. *Tectonophysics*, **226**, 113–141.

Goldhammer, R. & Harris, M. 1989. Eustatic controls on the stratigraphy and geometry of the Latemar buildup (Middle Triassic), the Dolomites of northern Italy. *In*: Crevello, P.D., Wilson, J.L., Sarg, J.F. & Read, J.F. (eds) *Controls on Carbonate Platform and Basin Development*. Society of Economic Palaeontologists, Special Publications, **44**, 323–338.

Goldhammer, R., Harris, M., Dunn, P. & Hardie, L. 1993. Sequence Stratigraphy and system tract development of the Latemar platform, Middle Triassic of the Dolomites (northern Italy): Outcrop calibration keyed by cycle stacking patterns. *In*: Loukes, R.G. & Sarg, J.F. (eds) *Carbonate Sequence Stratigraphy Recent Developments and Applications*. American Association of Petroleum Geologists, Memoirs, **57**, 353–387.

Hardebol, N.J. & Bertotti, G. 2013. DigiFract: A software and data model implementation for flexible acquisition and processing of fracture data from outcrops. *Computer and Geoscience*, **54**, 326–336.

Harris, M. 1994. The foreslope and toe-of-slope facies of the Middle Triassic Latemar buildup (Dolomites, northern Italy). *Journal of Sedimentary Research*, **64**, 132–132.

Hui, M., Kamath, J., Narr, W., Gong, B. & Fitzmorris, R. 2007. Realistic modeling of fracture networks in a giant carbonate reservoir. Paper SPE 11386, presented at the International Petroleum Technology Conference, 4–6 December 2007, Dubai, U.A.E.

Iverson, W. 1992. Fracture identification from well logs. Paper SPE 24351, presented at the SPE Rocky Mountain Regional Meeting, 18–21 May 1992, Casper, Wyoming.

Kasiri, N. & Bashiri, A. 2011. Status of dual-continuum models for naturally fractured reservoir simulation. *Petroleum Science and Technology*, **29**, 1236–1248.

Kazemi, H., Gilman, J. & Elsharkawy, A. 1992. Analytical and numerical solution of oil recovery from fractured reservoirs with empirical transfer functions. *SPE Reservoir Engineering*, **7**, 219–227.

Kfoury, M., Ababou, R., Noetinger, B. & Quintard, M. 2006. Upscaling fractured heterogeneous media: Permeability and mass exchange coefficient. *Journal of Applied Mechanics*, **73**, 41–46.

Klimczak, C., Schultz, R.A., Parashar, R. & Reeves, D.M. 2010. Cubic law with aperture–length correlation: Implication for network scale fluid flow. *Hydrogelogy Journal*, **18**, 851–862.

Kozubowski, T., Meerschaert, M. & Gustafson, G. 2008. A new stochastic model for fracture transmissivity assessment. *Water Resource Research*, **44**, W02435, http://dx.doi.org/10.1007/10.1029/2007WR006053.

Laubach, S., Olson, J. & Gross, M. 2009. Mechanical and fracture stratigraphy. *American Association of Petroleum Geologists Bulletin*, **93**, 1413–1426.

Li, B., Hoang, P., Mai, B. & Marie, L. 2011. Fracture characterization using borehole image logs and seismic data to define a successful drilling target in the fractured basement-a case study from the Nam Con Son Basin, southern offshore Vietnam. Paper 15300, presented at the International Petroleum Technology Conference, 7–9 February 2012, Bangkok, Thailand.

Makel, H. 2007. The modeling of fractured reservoirs: Constraints and potential for fracture network geometry and hydraulics analysis. *In*: Jolley, S.J., Barr, D., Walsh, J.J. & Knipe, R.J. (eds) *Structurally Complex Reservoirs*. Geological Society, London, Special Publications, **292**, 375–403.

Manrique, E., Muci, V. & Gurfinkel, M. 2007. EOR field experiences in carbonate reservoirs in the United States. *SPE Reservoir Evaluation & Engineering*, **10**, 667–686.

Marangon, A., Gattolin, G., Porta, G. & Preto, N. 2011. The Latemar: A flat-topped, steep fronted platform dominated by microbialites and synsedimentary cements. *Sedimentary Geology*, **240**, 97–114.

Mauldon, M. 1994. Intersection probabilities of impersistent joints. *International Journal of Rock Mechanics and Mining Sciences & Geomechanics Abstracts*, **31**, 107–115.

Meurer, M., Landis, L. & Lyons, S. 2005. Fracture network modeling and dual-permeability simulation of carbonate reservoirs. Paper 10954, presented at the International Petroleum Technology Conference, 21–23 November 2005, Doha, Qatar.

Moinfar, A., Narr, W., Hui, M., Mallison, B. & Lee, S. 2011. Comparison of discrete-fracture and dual-permeability models for multiphase flow in naturally fractured reservoirs. Paper SPE 142295, presented at the SPE Reservoir Simulation Symposium, 21–23 February 2011, The Woodlands, Texas, USA.

Namba, T. & Hiraoka, T. 1995. Capillary force barriers in a carbonate reservoir under waterflooding. Paper SPE 29773, presented at the Middle East Oil Show, 11–14 March 1995, Bahrain.

Nardon, S., Marzorati, D., Bernasconi, A. *et al.* 1991. Fractured carbonate reservoir characterization and modeling: A multidisciplinary case study from the Cavone oil field, Italy. *First Break*, **9**, 553–565.

Narr, W., Fischer, D., Harris, P., Heidrick, T., Robertson, B. & Payrazyan, K. 2008. Understanding and predicting fractures at Tengiz – a giant, naturally fractured reservoir in the Caspian Basin of Kazakhstan. *American Association of Petroleum Geologists*, Search and Discovery Article, 20057, http://www.searchanddiscovery.com/documents/2008/08041narr/images/narr.pdf.

Niemi, A., Kontio, K., Kuusela-Lahtinen, A. & Poteri, A. 2000. Hydraulic characterization and upscaling of fracture networks based on multiple-scale well test data. *Water Resources Research*, **36**, 3481–3497.

Oda, M. 1985. Permeability tensor for discontinuous rock masses. *Geotechnique*, **35**, 483–495.

Odling, N., Gillespie, P., Bourgine, B. *et al.* 1999. Variations in fracture system geometry and their implications for fluid flow in fractures hydrocarbon reservoirs. *Petroleum Geoscience*, **5**, 373–384.

Parra, J., Hackert, C., Bennett, M. & Collier, H. 2003. Permeability and porosity images based on nmr, sonic, and seismic reflectivity. *The Leading Edge*, **22**, 1102–1108.

Philip, Z., Jennings, J., Olson, J., Laubach, S. & Holder, J. 2005. Modeling coupled fracture–matrix fluid flow in geomechanically simulated fracture networks. *SPE Reservoir Evaluation and Engineering*, **8**, (4), 300–309.

Portella, R.C.M. & Prais, F. 1999. Use of automatic history matching and geostatistical simulation to improve production forecast. Paper SPE 53976, presented at the Latin American and Caribbean Petroleum Engineering Conference, 21–23 April 1999, Caracas, Venezuela.

Preto, N., Franceschi, M., Gattolin, G. *et al.* 2011. The Latemar: A Middle Triassic polygonal fault-block platform controlled by synsedimentary tectonics. *Sedimentary Geology*, **234**, 1–18.

Rantitsch, G. 1997. Thermal history of the Carnic Alps (Southern Alps, Austria) and its palaeogeographic implications. *Tectonophysics*, **272**, 213–232.

Rodriguez, A., Klie, H., Sun, S., Gai, X., Wheeler, M., Florez, H. & Simon, U. 2006. Upscaling of hydraulic properties of fractured porous media: Full permeability tensor and continuum scale simulations. Paper SPE 100057, presented at the SPE/DOE Symposium on Improved Oil Recovery, 22–26 April 2006, Tulsa, Oklahoma, USA.

Ruvo, L., Aldegheri, A., Galimberti, R., Nembrini, E., Rossi, L. & Ruspi, R. 2003. Multi-disciplinary study of the heavy-oil reservoirs in the Armatella Field, Sicily. *Petroleum Geoscience*, **9**, 265–276.

Storti, F., Balsamo, F., Cappanera, F. & Tosi, G. 2011. Sub-seismic scale fracture pattern and in situ permeability data in the chalk atop of the Krempe salt ridge at Lägerdorf, NW Germany: Inferences on synfolding stress field evolution and its impact on fracture connectivity. *Marine and Petroleum Geology*, **28**, 1315–1332.

Subbey, S., Christie, M. & Sambridge, M. 2002. Uncertainty reduction in reservoir modelling. *Contemporary Mathematics*, **295**, 457–468.

Underwood, C., Cooke, M., Simo, J. & Muldoon, M. 2003. Stratigraphic controls on vertical fracture patterns in Silurian dolomite, northeastern Wisconsin. *American Association of Petroleum Geologists Bulletin*, **87**, 121–142.

Visona, D. 1997. The Predazzo multiple intrusive body (Western Dolomites, Italy). Field and mineralogical studies. *Memorie di Scienze Geologiche*, **49**, 117–122.

Wang, X. 2005. *Stereological interpretation of rock fracture traces on borehole walls and other cylindrical surfaces*. PhD thesis, Virginia Polythechnic Institute and State University.

Waren, J. & Root, P. 1963. The behaviour of naturally fractured reservoirs. *SPE Journal*, **3**, 245–255.

Wennberg, O., Svana, T., Azizzadeh, M., Aqrawi, A., Brockbank, P., Lyslo, K. & Ogilvie, S. 2006. Fracture intensity vs. mechanical stratigraphy in platform top carbonates: The Aquitanian of the Asmari Formation, Khaviz Anticline, Zagros, SW Iran. *Petroleum Geoscience*, **12**, 235–246.

Whiterspoon, P., Wang, J., Iwai, K. & Gale, J. 1980. Validity of cubic law for fluid flow in a deformable rock fracture. *Water Resources Research*, **16**, 1016–1024.

Yose, L., Brown, S., Davis, T., Eiben, T., Kompanik, G. & Maxwell, S. 2001. 3D geologic model of a fractured carbonate reservoir, Norman Wells Field, NWT, Canada. *Bulletin of Canadian Petroleum Geology*, **49**, 86–116.

Received 24 January 2013; revised typescript accepted 13 October 2013.